



HAL
open science

Ductilisation and fatigue life enhancement of selective laser melted AlSi10Mg by friction stir processing

Juan Guillermo Santos Macías, Chola Elangeswaran, Lv Zhao, Brecht van Hooreweder, Jérôme Adrien, Éric Maire, Jean-Yves Buffiere, Wolfgang Ludwig, Pascal Jacques, Aude Simar

► To cite this version:

Juan Guillermo Santos Macías, Chola Elangeswaran, Lv Zhao, Brecht van Hooreweder, Jérôme Adrien, et al.. Ductilisation and fatigue life enhancement of selective laser melted AlSi10Mg by friction stir processing. *Scripta Materialia*, 2019, 170, pp.124-128. 10.1016/j.scriptamat.2019.05.044 . hal-02271543

HAL Id: hal-02271543

<https://hal.science/hal-02271543>

Submitted on 2 Jun 2022

HAL is a multi-disciplinary open access archive for the deposit and dissemination of scientific research documents, whether they are published or not. The documents may come from teaching and research institutions in France or abroad, or from public or private research centers.

L'archive ouverte pluridisciplinaire **HAL**, est destinée au dépôt et à la diffusion de documents scientifiques de niveau recherche, publiés ou non, émanant des établissements d'enseignement et de recherche français ou étrangers, des laboratoires publics ou privés.

Ductilisation and fatigue life enhancement of selective laser melted AlSi10Mg by friction stir processing

Juan Guillermo Santos Macías^{a,*}, Chola Elangeswaran^b, Lv Zhao^a, Brecht Van Hooreweder^b, Jérôme Adrien^c, Eric Maire^c, Jean-Yves Buffière^c, Wolfgang Ludwig^c, Pascal J. Jacques^a, Aude Simar^a

^a*Université catholique de Louvain, Institute of Mechanics, Materials and Civil Engineering, IMAP, B-1348 Louvain-la-Neuve, Belgium*

^b*Department of Mechanical Engineering, KU Leuven, Celestijnenlaan 300b, B-3001 Leuven, Belgium*

^c*Université de Lyon, Mateis, INSA Lyon, UMR5510 CNRS, F-69621 Villeurbanne, France*

*Corresponding author.

E-mail address: juan.santos@uclouvain.be

Abstract

In the effort of expanding the already existing applications of additively manufactured parts, improving mechanical performance is essential. Friction stir processing (FSP) is a promising post-treatment solution to tackle this issue. FSP of selective laser melted AlSi10Mg leads to the globularisation of the Si-rich eutectic network, microstructural homogenisation and porosity reduction. These features have been characterised using in and ex situ mechanical testing and different imaging techniques. A significant modification of the damage mechanism is reported with an increase of the fracture strain from 0.1 to 0.4 after FSP and an enhancement over two orders of magnitude in fatigue life.

Keywords:

Selective laser melting

Friction stir processing

Aluminium alloys

Ductility

Fatigue test

Additive manufacturing (AM) has opened many opportunities for structural design and optimisation in several sectors, including aerospace, automotive and medical applications. AM offers more design opportunities, flexibility and material saving features [1]. Despite these potential advantages, there are also limitations related to the nature or the novelty of the technology, such as microstructural inhomogeneity and the presence of porosity. These specific shortcomings restrain the use of metal AM in structural components. In particular, the severe requirements imposed by the aerospace industry, notably in terms of damage and fatigue resistance, are not yet met satisfactorily immediately after the AM process. These poor performances are reported to be mainly due to microstructural inhomogeneity and excessive porosity [2].

In order to tackle these issues, several approaches are possible, such as new alloy development or optimisation of manufacturing parameters. Post-treatments also play an important role and are often necessary to reach the required mechanical performances. They range from heat treatments to reduce residual stress [3] or to homogenise the microstructure [4], to surface finishing techniques to decrease roughness and thus to enhance fatigue resistance [2].

Other processing stages can be seen as particularly suitable solutions. One of them is hot isostatic pressing (HIP), which combines high pressure and elevated temperature to efficiently reduce porosity. The HIP process is now successfully implemented in the manufacturing strategy of AM Ti6Al4V parts [5]. Nevertheless, the use of the HIP technique also presents strong limitations. The relatively long time spent at high temperature during the HIP process ultimately coarsens the AM microstructure, leading to poor strength. Furthermore, the application of a HIP stage does not seem to bring any beneficial influence on AM AlSi10Mg parts [6-10], motivating the quest for new post-treatments.

The present work shows that friction stir processing (FSP) can be used for improving the mechanical behaviour of AM parts, particularly in the case of AlSi10Mg alloy processed by selective laser melting (SLM). FSP is derived from friction stir welding [11]. Using a rotating non-consumable cylindrical tool composed of a shoulder with a pin at the tip that penetrates through the material, a local thermomechanical treatment is applied, bringing microstructural changes such as particle breakdown and redistribution, homogenisation or refinement [11]. FSP can be applied locally in regions of stress concentration of critical parts.

FSP has been shown as a very effective way of improving mechanical behaviour in several materials, including cast [12-15] and wrought [16] Al alloys and Ti alloys [17]. For instance, huge improvement of ductility (i.e. increase of the elongation at failure from 0.01 before FSP to 0.15 after FSP) together with a fivefold increase of fatigue life have been reported after performing FSP on an F357 cast alloy (a hypoeutectic Al-Si alloy), while maintaining the yield strength and enhancing the ultimate tensile strength by 10% [14]. Hannard et al. [16] demonstrated the ductility enhancement brought about by FSP thanks to its ability to break down and redistribute Fe-rich intermetallic particles. However, its use on AM parts has only been reported by Ref. [18,19] for AlSi10Mg, where the authors essentially studied the influence of FSP on several microstructural features, observing promising microstructural homogenisation, and by Huang et al. [20] for Ti6Al4V, in which ductility was increased due to the elimination of the brittle phase by FSP. The nature of FSP, characterised by a short heat exposure time, avoiding microstructure coarsening, is thus expected to improve mechanical performances of SLM AlSi10Mg.

SLM AlSi10Mg 150x35x5 mm plates were manufactured using an EOS M290 set-up with standard optimised parameters (Laser power = 390 W; layer thickness = 30 μm ; hatch spacing = 0.19 mm; scanning speed = 1300 mm/s; scan rotation = 67°). Plates were manufactured with a build platform temperature of 35 °C. It is worth mentioning that using a higher build platform temperature during the SLM process decreases residual stresses, which can be problematic during the manufacturing process (causing part deformation and manufacturing interruption), but using higher temperature also leads to lower post-manufacturing strength. Therefore, to minimise the effect of residual stress, a stress relief heat treatment (SRHT) at 300 °C for 2 h, was performed under Ar atmosphere on some samples after the AM process. These SRHT samples were used for comparison purposes. To study the effect of FSP post-treatment on SLM processed AlSi10Mg, FSP was performed on some as built (AB) samples using a Hermle UWF 1001 H milling machine at a rotational speed of 1000 rpm and a traverse speed of 500 mm/min.

Fig. 1a-c illustrate key microstructural features of AB, SRHT and FSP samples. The characteristic Si-rich eutectic interconnected network surrounding the α -Al phase of AB microstructure (Fig. 1a) is clearly broken down after FSP as presented on Fig. 1c. In both the SRHT (Fig. 1b) and FSP (Fig. 1c) samples, the Si-rich eutectic phase becomes more globular, but the very fine nature of the microstructure is preserved. Regarding the fine Si precipitates found inside the α -Al cells of the AB material [21], observable on Fig. 1a, their evolution is different after SRHT and FSP treatments. While the SRHT seems to increase their size, the fraction and number of these fine particles are lower in the FSP material. This could be due to a solutionising effect induced by the temperatures reached during FSP, which can be of the order of 80% of the melting temperature of the Al alloys [11]. Indeed, a thermocouple introduced in the centre of the FSP tool 3 mm above the shoulder gave a reading of 447 °C during the course of FSP suggesting a temperature above 500°C in the processed material. Thus, the SRHT, only reaching 300 °C, remains significantly lower than the solutionising temperature.

X-ray tomography measurements were performed at the European Synchrotron Radiation Facility (ESRF) ID11 beamline (Grenoble, France) on specimens extracted from AB, SRHT and FSP plates. The voxel size was 0.75 μm . In the final analysis porosities presenting volumes smaller than 3 voxels (i.e. $\varnothing_{\text{eq}} \leq 1.3 \mu\text{m}$) were rejected from the population. Comparison of Fig. 1d, e and f illustrates the decrease of the proportion of observable porosities from about 0.13% for the AB and SRHT samples to 0.03% for the FSP sample. In the context of fatigue resistance enhancement, it is worth noting that the most important effect of FSP is the

complete elimination of the larger porosities, which can reach up to $\varnothing_{eq} = 50 \mu\text{m}$. Indeed, after FSP the remaining porosity has an equivalent diameter below $10 \mu\text{m}$. The volume fraction of porosity larger than $5 \mu\text{m}$ equivalent diameter is about 0.09% for AB and SRHT and 0.02% for FSP. Furthermore, large Fe-rich intermetallic particles that may act as damage nucleation sites were found to be broken down and dispersed, which is also expected to be beneficial for ductility enhancement [16].

Uniaxial tensile tests were performed following ASTM E8 / E8M - 15a standard. Horizontally oriented round tensile specimens were extracted by machining from the AB plates and from the FSP region. Fig. 2 presents the true stress - true strain curves of the three states. Continuous lines correspond to the uniform deformation of the specimens up to necking, which is observable on FSP and SRHT specimens, but not on AB ones. The deformation at fracture, estimated by the final size of the fractured sample ($\epsilon_f = \ln(A_0 / A_f)$) and the final force applied ($\sigma_f = F_f / A_f$), are represented with a cross. The post-necking tensile behaviour of the FSP and SRHT samples until fracture are estimated using a linear extrapolation.

All samples fulfil the Considère criterion. FSP results in a decrease of the strength level. Nevertheless, the FSP material presents similar yield and ultimate tensile strength levels to the SRHT material, thus showing a satisfactory mechanical behaviour. SRHT samples show more strain hardening at an earlier stage that could be attributed to more dislocation storage by the Orowan mechanism due to the fine ($\varnothing_{eq} \approx 100 \text{ nm}$) Si-rich precipitates observed on Fig. 1b [22,23]. A significant improvement is observed in the fracture strain of SRHT and FSP samples. They present a fourfold increase in fracture strain (ϵ_f) compared to the SLM AB material. Taking into account the necessary compromise between strength, uniform elongation, ductility and residual stress relief, these treatments can be considered as significantly positive.

The fracture strain enhancement provided by SRHT and FSP compared to AB samples can be related to the significant changes of the micro and mesostructures. The damage mechanisms were analysed using SEM imaging along the longitudinal plane (i.e. section at mid-thickness along the loading direction) of tensile samples after failure (Fig. 3a-c). The observation of the damaged area close to the fracture surface reveals differences depending on the processing conditions. Damage originates predominantly through fracture of the Si-rich eutectic network for the AB material, as depicted on Fig. 3a. In the FSP and SRHT samples, damage is also related to the Si-rich eutectic phase, but it consists of both Si-rich particle fracture and particle-matrix decohesion (Fig. 3b for SRHT and Fig. 3c for FSP). Furthermore, damage events are more numerous and larger voids are observed on the FSP material, due to larger deformation before failure allowing more cavity growth.

At a mesostructural level, the melt pool boundaries seem to have a negative effect on the mechanical behaviour. This can be observed on Fig. 3d, which shows that the crack leading to failure partially followed a melt pool boundary. As more void nucleation occurs in the coarser microstructure within the reheated regions of the melt pool boundaries, the crack tends to preferentially follow these zones. These boundaries are reported as being softer [24] and thus experiencing deformation localisation. Therefore, damage concentrates in these regions leading to more nucleation of cavities in the Si-rich eutectic phase network. FSP eliminates the melt pool structure and the differentiated zones, thus bringing an homogenisation effect at the mesostructural level. Indeed, Fig. 3e shows that melt pools apparent on the right side of the figure, unaffected by the FSP process, have disappeared in the FSP zone.

Final fracture results from the succession of damage mechanisms involving nucleation of cavities on Si-rich particles, their growth and coalescence. In the AB sample, the Si-rich interconnected network acts as a source of numerous nucleation sites for cavities. This brittle network breaks down with increasing strain since it cannot follow the α -Al matrix deformation, which is more ductile. FSP and SRHT lead to a globularisation of this network. Thus, the behaviour of these samples is expected to be driven by the ductile aluminium network that can now deform more to accommodate external loading, allowing for higher ductility.

Fatigue testing was performed following ASTM E466 - 15 standard (force controlled constant amplitude). Tensile - tensile tests ($R = 0.1$) with a frequency of 45 Hz were carried out on an Instron E10000 stress rig.

Specimens were polished down to an arithmetic roughness $R_a < 0.1 \mu\text{m}$ in order to get rid of any surface state related effects. Table 1 gives a fatigue life comparison between AB, SRHT and FSP samples tested at a stress level of 250 MPa, i.e. slightly above the yield strength of the SRHT and FSP specimens and lower than the one of the AB samples. Slight strain hardening effects are thus expected [25]. SRHT state is used as a reference in addition to the AB state since it presents a similar yield strength to the FSP state. Tests were conducted up to a maximum of 10^7 cycles. These results show that FSP samples have a fatigue life up to at least two orders of magnitude longer than AB or SRHT ones.

Although SRHT brings a similar level of ductilisation to FSP, the fatigue life is much shorter for the former condition. This suggests that porosity plays a predominant role over the microstructure on fatigue resistance. The relative density of the material is satisfactory, being well above 99.5%. However, the presence of pores of a size larger than the very fine microstructure obtained after the SLM process becomes a critical factor. The large porosities found at surface or subsurface level act as fatigue crack nucleation sites. This can be appreciated through fractography analysis of the fractured fatigue samples. Fatigue cracks were found to systematically originate on sub-surface defects for AB and SRHT materials, as extensively described in the literature [2,26,27].

Low cycle fatigue testing of continuous radius samples was performed in various steps interrupted by X-ray tomography observations (i.e. ex situ). These observations were also performed at ESRF ID11 beamline. The samples had a curvature radius $r = 2.5 \text{ mm}$, a minimum diameter of $\varnothing_{\text{min}} \approx 1 \text{ mm}$, and were polished with 1200 grit SiC paper down to an $R_a \approx 1.5 \mu\text{m}$. They were tested at a maximum stress of 195 MPa and a stress ratio of 0.15. Compared to the tests reported in Table 1, the samples used for these ones had a rougher surface and a geometry leading to a higher triaxiality, justifying the lower applied maximum stress. Tomography allows monitoring the fatigue crack growth, which occurs under mode I (Fig. 4). To obtain the data for this figure, the voxels belonging to the cracks are projected onto a plane perpendicular to the loading direction. This results in a projected view of the crack, allowing to measure its length (i.e. maximum depth of the crack front). Fatigue crack nucleation is delayed after FSP while the final growth seems slightly affected. The elimination of the large porosities after FSP essentially acts on fatigue crack nucleation and is thus a decisive factor in the fatigue life improvement.

FSP on SLM AlSi10Mg alloy brings not only excellent ductility similar to SRHT material but also very significant fatigue life enhancement (see summary table on supplementary material). FSP leads to the breakdown of the Si-rich eutectic phase interconnected network, resulting in a drastic increase of ductility. FSP also leads to porosity reduction and elimination of the large defects that are the nucleation sites for fatigue cracks in AB or SRHT materials. FSP also eliminates the melt pool structure and the presence of heat affected zones in the contour of the melt pools. These inhomogeneities lead to strain localisation at melt pool boundaries, so the FSP process helps to mitigate this effect.

The benefits brought by FSP allow its postulation as a potentially viable post-treatment for SLM AlSi10Mg and other AM parts in general. As a local surface treatment, its use can be recommended for parts presenting specific zones submitted to high mechanical loads, e.g. zones of stress concentration. Considering that these parts (or specific zones alone) are to go through a final machining or surface finishing step to avoid poor fatigue resistance derived from low surface quality, a good practice would be to implement FSP just before machining. It can be carried out in a milling machine or machining centre, in the same manufacturing step, in contrast to other potential methods, such as HIP, which would need an extra step.

Acknowledgements

The authors would like to thank the ESRF for allocation of beam time at ID11 (experiment number MA3758). JGSM acknowledges the support of the Fonds de la recherche scientifique - FNRS (FRIA grant), Belgium. This research has also been funded (from January 2017) by the European Research Council (ERC) under the European Union's Horizon 2020 research and innovation program (grant agreement n°716678). Any-Shape is acknowledged for material supply.

References

- [1] M.K. Thompson, G. Moroni, T. Vaneker, G. Fadel, R.I. Campbell, I. Gibson, A. Bernard, J. Schulz, P. Graf, B. Ahuja, F. Martina, *CIRP Annals - Manuf. Technol.* 65 (2) (2016) 737–760.
- [2] T.M. Mower, M.J. Long, *Mater. Sci. and Eng. A* 651 (2016) 198–213.
- [3] EOS GmbH - electro optical systems, Material data sheet for EOS Aluminium AlSi10Mg. München, 2014.
- [4] E. Brandl, U. Heckenberger, V. Holzinger, D. Buchbinder, *Mater. and Des.* 34 (2012) 159–169.
- [5] M. Qian, W. Xu, M. Brandt, H. Tang, *MRS Bull.* 41 (10) (2016) 775–784.
- [6] I. Rosenthal, E. Tiferet, M. Ganor, A. Stern, *Annals of Dunarea de Jos University of Galati* 12 (26) (2015) 33–38.
- [7] N. Uzan, R. Schneck, O. Yeheskel, N. Frage, *Mater. Sci. and Eng. A* 704 (2017) 229–237.
- [8] I. Rosenthal, R. Schneck, A. Stern, *Mater. Sci. and Eng. A* 729 (2018) 310–322.
- [9] F. Trevisan, F. Calignano, M. Lorusso, J. Pakkanen, A. Aversa, E.P. Ambrosio, M. Lombardi, P. Fino, D. Manfredi, *Mater.* 10 (1) (2017) 76.
- [10] N. Larrosa, W. Wang, N. Read, M.H. Loretto, C. Evans, J. Carr, U. Tradowsky, M. Attallah, P. Withers, *Theoretical and Appl. Fract. Mech.* 98 (2018) 123–133.
- [11] R.S. Mishra, Z.Y. Ma, *Mater. Sci. and Eng. R* 50 (2005) 1–78.
- [12] Z.Y. Ma, S.R. Sharma, R.S. Mishra, M.W. Mahoney, *Mater. Sci. Forum* 426–432 (2003) 2891–2896.
- [13] S.R. Sharma, Z.Y. Ma, R.S. Mishra, *Scr. Mater.* 51 (3) (2004) 237–241.
- [14] S. Jana, R.S. Mishra, J.B. Baumann, G. Grant, *Acta Mater.* 58 (2010) 989–1003.
- [15] S. Jana, R.S. Mishra, J.A. Baumann, G.J. Grant, *Metall. Mater. Trans. A* 41 (10) (2010) 2507–2521.
- [16] F. Hannard, A. Simar, E. Maire, T. Pardoën, *Acta Mater.* 148 (2018) 456–466.
- [17] J. Su, J. Wang, R.S. Mishra, R. Xu, J.A. Baumann, *Mater. Sci. And Eng. A* 573 (2013) 67–74.
- [18] A.H. Maamoun, S.C. Veldhuis, M. Elbestawi, *J. of Mater. Process. Technol.* 263 (2019) 308–320.
- [19] T. Yang, K. Wang, W. Wang, P. Peng, L. Huang, K. Qiao, Y. Jin, *JOM* (2019) 1–11.
- [20] C. Huang, X. Yan, L. Zhao, M. Liu, W. Ma, W. Wang, J. Soete, A. Simar, *Mater. Sci. and Eng. A* 755 (2019) 85–96.
- [21] J. Wu, X.Q. Wang, W. Wang, M. Attallah, M.H. Loretto, *Acta Mater.* 117 (2016) 311–320.
- [22] Z. Zhang, D.L. Chen, *Scr. Mater.* 54 (2006) 1321–1326.
- [23] B. Chen, S.K. Moon, X. Yao, G. Bi, J. Shen, J. Umeda, K. Kondoh, *Scr. Mater.* 141 (2017) 45–49.
- [24] M. Tang, P.C. Pistorius, *JOM* 69 (3) (2017) 516–522.
- [25] R.F. Hanstock, *Proc. Phys. Soc.* 59 (1947) 275–287.
- [26] B. Zhang, D.R. Poirier, W. Chen, *Metall. Mater. Trans. A* 30 (10) (1999) 2659–2666.
- [27] S. Tammis-Williams, P.J. Withers, I. Todd, P.B. Prangnell, *Sci. Rep.* 7 (2017) 7308.

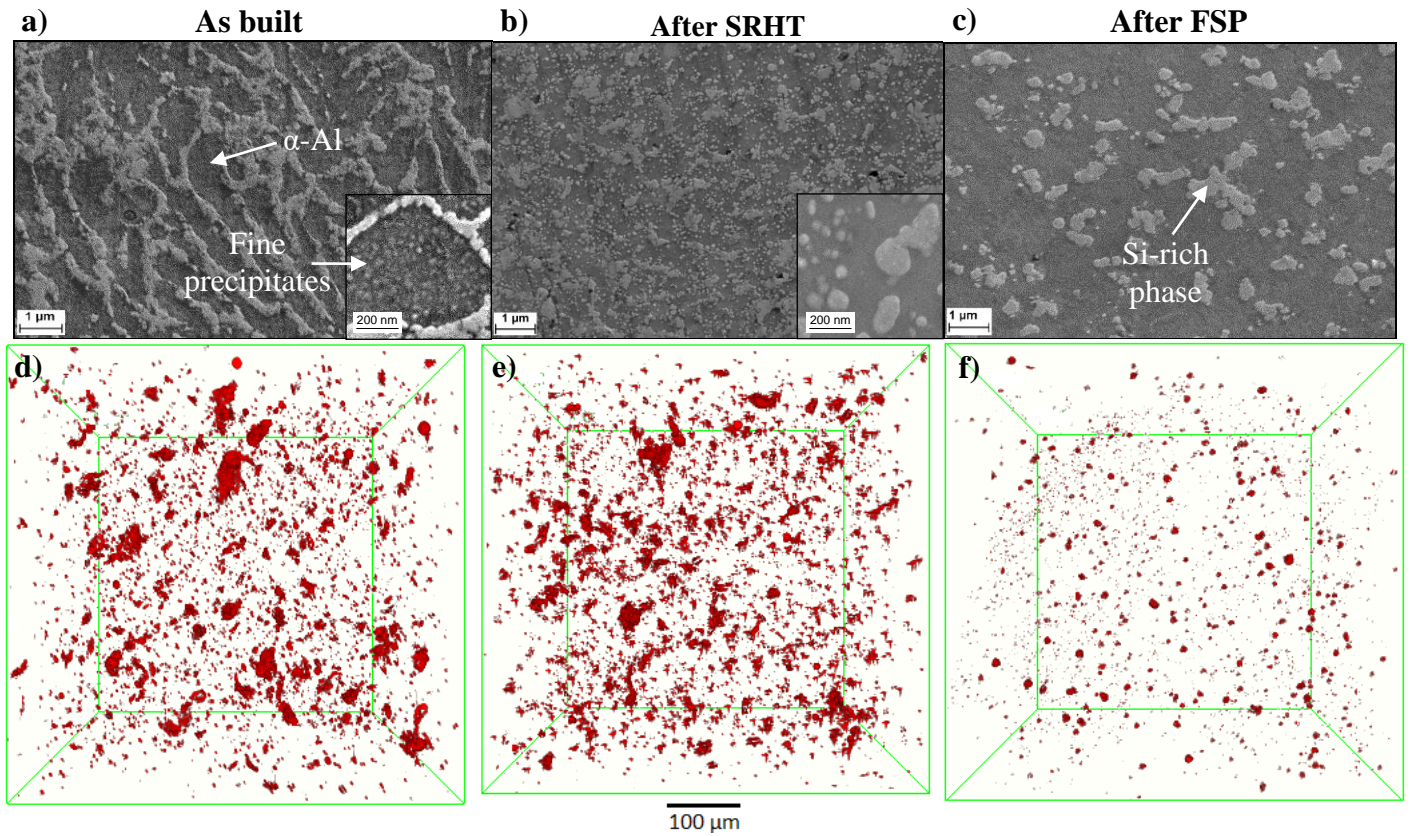


Fig. 1. SEM micrographs depicting the microstructural features and 3-D X-ray synchrotron tomography reconstructions showing porosity of SLM AlSi10Mg as built (a,d), after SRHT at 300 °C during 2 h (b,e) and after FSP at 1000 rpm rotational speed and 500 mm/min traverse speed (c,f)

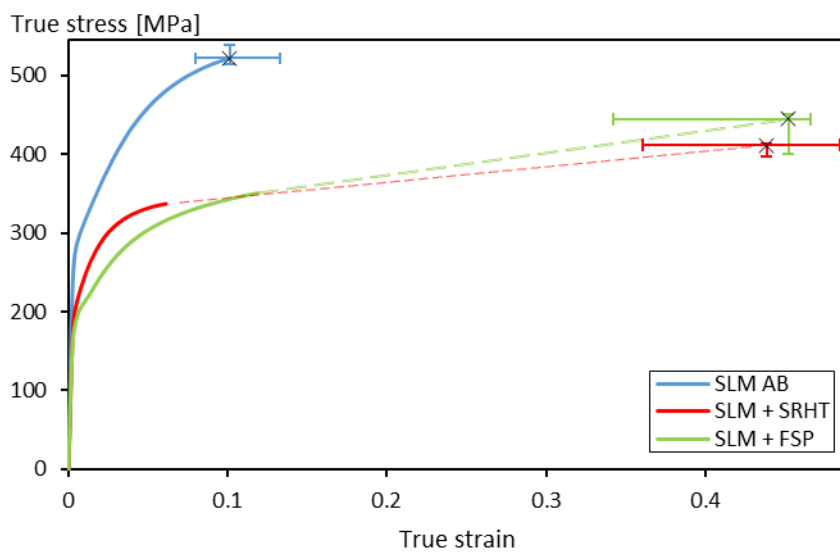


Fig. 2. Representative tensile true stress - true strain curves of SLM AlSi10Mg AB, SRHT and FSP (out of 6 tested samples for AB and 3 for SRHT and FSP)

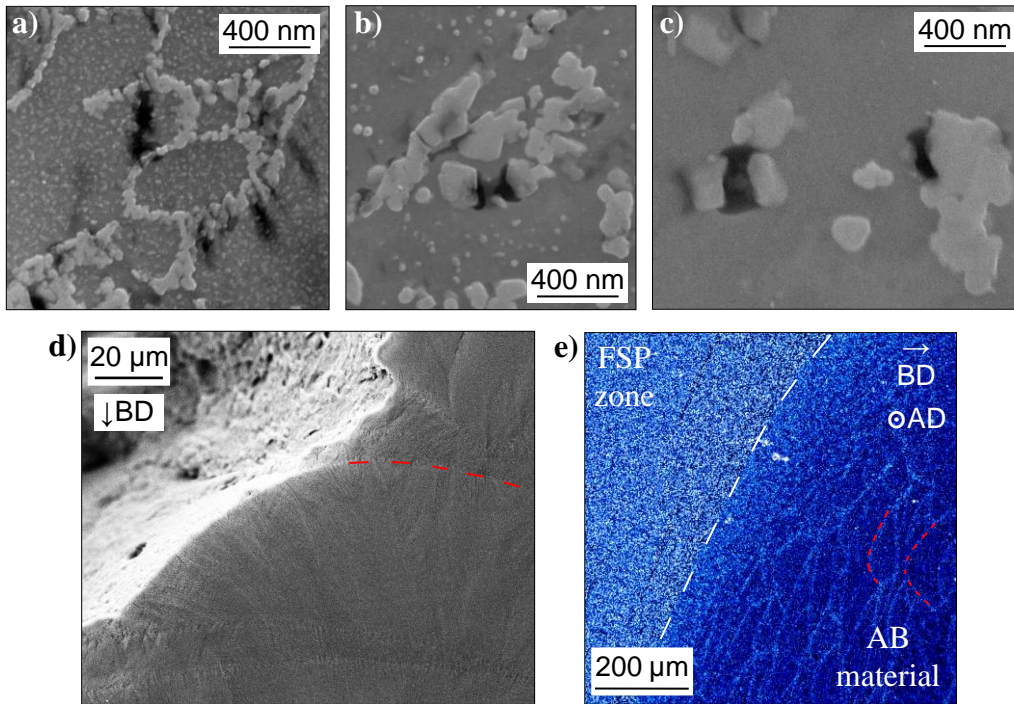


Fig. 3. SEM micrographs along longitudinal plane on SLM AlSi10Mg a) as built tensile specimen after failure, showing damage nucleation on the Si-rich eutectic network, b) SRHT and c) FSP tensile sample after failure, showing damage nucleation on Si-rich eutectic phase and decohesion of Si particles and Al matrix; d) SEM in situ tensile testing micrograph of an as built sample showing final failure crack following a melt pool boundary; and e) FSP sample light optical microscope micrograph with melt pools apparent outside the FSP area (BD = Building direction; AD = Advancing direction of FSP tool)

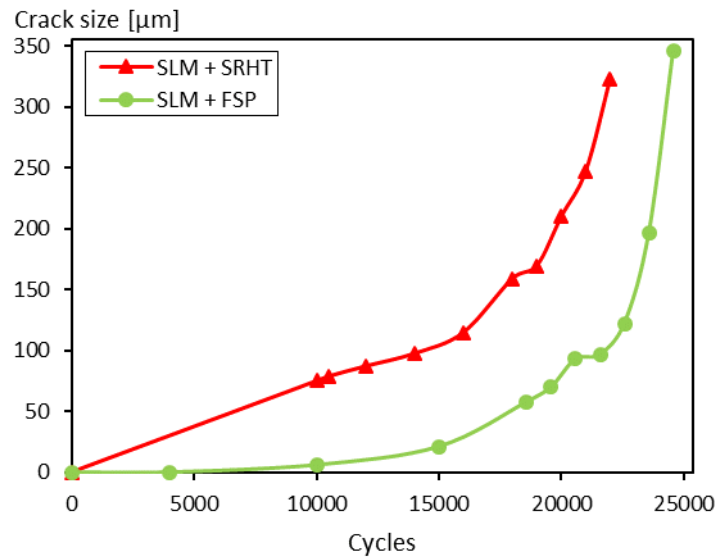


Fig. 4. Fatigue crack growth data obtained from the X-ray tomographic images for 2 material conditions

Table 1

Fatigue testing data for SLM AlSi10Mg AB and after SRHT or FSP (2 tests per state)

State	Max stress [MPa]	Min stress [MPa]	Cycles to failure
AB	250	25	$7.6-10.1 \cdot 10^4$
SRHT	250	25	$6.6-8.0 \cdot 10^4$
FSP	250	25	No failure after $5.5-10.0 \cdot 10^6$

Supplementary Table 1

Porosity, tensile properties and fatigue life for SLM AlSi10Mg AB and after SRHT or FSP. σ_y represents the yield strength, UTS represents the ultimate tensile strength, ε_f represents the fracture strain.

	Porosity (%)	σ_y [MPa]	UTS [MPa]	ε_f	Fatigue cycles to failure at $\sigma_{max} 250$ MPa R0.1
AB	0.13	287±2	473±2	0.1±0.03	$7.6-10.1 \cdot 10^4$
SRHT	0.13	212±12	319±16	0.42±0.06	$6.6-8.0 \cdot 10^4$
FSP	0.03	189±5	312±8	0.4±0.06	No failure after $5.5-10.0 \cdot 10^6$